STATE RESEARCH CENTER OF RUSSIA

INSTITUTE FOR HIGH ENERGY PHYSICS

IHEP 96-104

L.G. Landsberg

SEARCH FOR EXOTIC BARYONS IN THE EXPERIMENTS ON PROTON BEAM WITH E_p=70 GeV AND OTHER MEASUREMENTS WITH THE SPHINX FACILITY

The SPHINX Collaboration

The extended version of the invited talk at the XIX Workshop on High Energy Physics and Field Theory, IHEP, Protvino, June 25-28, 1996.

Protvino 1996

UDK 681.3.06.069 M–24

Abstract

Landsberg L.G. Search for Exotic Baryons in the Experiments on Proton Beam with Energy E_p = 70 GeV and Other Measurements with the SPHINX Facility : IHEP Preprint 96-104. – Protvino, 1996. – p. 48, figs. 36, tables 3, refs.: 72.

In this review the results of the first stage of the experiments with the SPHINX facility are presented. In these experiments several diffractive production processes in a 70 GeV proton beam of the IHEP accelerator were studied. The evidence for new baryon states with masses $\geq$ 2 GeV is obtained in the hyperon-kaon effective mass spectra in the coherent reactions $p + C \to [\Sigma(1385)^0 K^+] + C$ and $p + C \to [\Sigma^0 K^+] + C$. The unusual features of these massive states (small enough decay widths, large branching ratios for decays with strange particles in final states) make them serious candidates for cryptoexotic pentaquark baryons with hidden strangeness. Preliminary data for $p + N$ reactions in nonperiferal region with transverse momenta square > 0.3 GeV^2 (the mass spectra $M(\Sigma^0 K^+)$, $M(p\eta)$ and $M(p\eta')$) are also presented in this review.

Аннотация

Ландсберг Л.Г. Поиски экзотических барионов в экспериментах на протонном пучке с энергией 70 ГэВ и другие измерения на установке СФИНКС: Препринт ИФВЭ 96-104. – Протвино, 1996. – 48 с., 36 рис., 3 табл., библиогр.: 72.

В настоящем обзоре суммируются результаты первого этапа исследований процессов дифракционного образования частиц протонами с энергией 70 ГэВ, проводившихся на установке СФИНКС. При анализе спектров эффективных масс гиперон-каонных систем в когерентных реакциях $p + C \to [\Sigma(1385)^0 K^+] + C$ и $p + C \to [\Sigma^0 K^+] + C$ на ядрах углерода получены данные о существовании новых барионных состояний с массами $\geq$ 2 ГэВ. Необычные свойства этих массивных состояний (сравнительно узкая ширина, аномально большие вероятности распада по каналам с образованием странных частиц в конечных состояниях) делают их серьёзными кандидатами в криптоэкзотические пентакварковые барионы со скрытой странностью. Приводятся также первые результаты, связанные с исследованиями непериферических процессов образования частиц в области $P_T^2 > 0.3$ GeV^2 (спектры масс $M(\Sigma^0 K^+)$, $M(p\eta)$ и $M(p\eta')$).

1. Introduction

A rapid development of the hadron spectroscopy in recent years has led to a significant advance in the systematics of "ordinary" hadrons with the simplest valence quark structure: $q\bar{q}$ for mesons and qqq for baryons. At the same time several unusual hadrons with some anomalous features have been found. They do not fit in the systematics of this simplest quark model and are interpreted as a new form of hadronic matter – exotic hadrons. These states can include multiquark formations ($qq\bar{q}\bar{q}$ mesons and $qqqq\bar{q}$ baryons), hybrid systems with valence quarks and gluons ($q\bar{q}g$ mesons and $qqqg$ baryons), or glueballs, i.e. mesons consisting solely of valence gluons (gg, ggg). The discovery of the exotic hadrons would have far-reaching consequences for quantum chromodynamics, for the concept of confinement and for specific models of hadron structure (lattice, string and bag models). Detailed discussions of exotic hadron physics can be found in recent reviews [1-7].

Exotic hadrons can have anomalous quantum numbers not accessible to three-quark baryons or quark-antiquark mesons (open exotic states), or even usual quantum numbers (cryptoexotic states). Cryptoexotic hadrons can be identified only by their unexpected dynamical properties (anomalously narrow decay widths, anomalous decay branching ratios and so on).

As is clear from review papers [1-7], in the last decade searches for exotic mesons have led to considerable advance in this field. Several new states have been observed whose properties cannot be explained in the framework of naive quark model of ordinary mesons with $q\bar{q}$ valence quark structure. These states are serious candidates for exotic mesons (most of them are of cryptoexotic type).

At the same time the situation for exotic baryons is far from being clear. There are also some examples of possible unusual baryon resonances [8-11], but these data are not sufficiently precise and are not supported by some new experimental results [2,12-16].

Extensive studies of the diffractive baryon production and search for cryptoexotic pentaquark baryons with hidden strangeness ($B_\phi = |qqqs\bar{s}>$, here $q = u, d$ quarks) are being carried out by the SPHINX Collaboration at the IHEP acceleratior with 70 GeV proton beam. This program was described in detail in reviews [2].

The recent data of the SPHINX experiment [16-21] gave new important evidence of possible existence of cryptoexotic baryons with hidden strangeness $X(2050)^+ \to \Sigma(1385)^0 K^+$ and $X(2000)^+ \to \Sigma^0 K^+$. We shall summarize these data in Sections 3-6, after a general description of the nature and expected properties of cryptoexotic baryons, as well as some promising ways for their production and observation. We shall also present here first data on the studying $p\eta$ and $p\eta'$ systems in proton-induced diffractive-type reactions and on possible new effects in nonperipheral domain for these processes (Sections 7 and 8, [20, 21]). Investigation of Λ^* hyperon resonances in isoscalar $\Sigma^0\pi^0$ system will be discussed in Section 9 and the results of studying the OZI selection rule in hadronic processes will be shown in Section 10 ([22-24]). After a short resume of earlier measurements on searching for heavy baryons with hidden strangeness [12] or with strong coupling with $p\bar{p}$ states [25] (see Section 11) we will present new data on neutral meson production in quasiexclusive proton reactions in the deep fragmentation region (Section 12, [26-28]). Some earlier results of the SPHINX experiments have been reviewed in more detailes in Ref.[2,16].

2. Cryptoexotic baryons

As has been stated before, cryptoexotic baryons do not have external exotic quantum numbers and their complicated internal valence structure can be established only indirectly, by examination of their unusual dynamic properties which are quite different from those for ordinary $|qqq>$ baryons. In this connection let us consider the properties of multiquark baryons with hidden strangeness $B_\phi = |qqqs\bar{s}> (q = u, d)$.

If such cryptoexotic baryon structure consists of two color parts separated in space with a centrifugal barrier, then its decays into the color singlet final states may be suppressed because of a complicated quark rearrangement in decay processes. The properties of multiquark exotic baryons with internal color structure

$$|qqqq\bar{q}>_{1c}= |(qqq)_{8c} \bigodot (q\bar{q})_{8c}> \tag{1}$$

(color octet bonds) or

$$|qqqq\bar{q}>_{1c}= |(qq\bar{q})_{\overline{6c}} \bigodot (qq)_{6c}> \tag{2}$$

(color sextet-antisextet bonds) are discussed in [29-32]. Here subscripts 1c, 8c and so on specify the representation of the color $SU(3)_c$ group. If the mass of a nonstrange baryon with hidden strangeness is above the threshold for the decay modes with the strange particles in final states, then the main decay channels should be of the type

$$B_\phi \to YK + k\pi \tag{3}$$

(k=0;1;...). Another possibility is associated with the decays

$$B_\phi \to \phi N(\eta N; \eta' N) + k\pi, \tag{4}$$

i.e. with emission of particles with a significant $s\bar{s}$ component in their valence quark structure. It must be also stressed that η and particularly η' mesons are strongly coupled with gluon fields and, then, with states with enriched gluon component. Therefore baryon decays of $B \to N\eta; N\eta'$ type may be the specific decay modes for the hybrid baryons (see, for example, reviews [2]).

The nonstrange decays of baryons with hidden strangeness $B_\phi \to N + n\pi$ must be suppressed by the OZI rule. Thus, the effective phase space factors for the decays of massive B_ϕ baryons would be significantly reduced because of this OZI suppression (owing to a large enough mass threshold for the allowed $B_\phi \to YK$ decays to be compared with suppressed $B_\phi \to N\pi; \Delta\pi$ ones). The mechanism of quark rearrangement of color clusters in the decay processes for the objects with complicated inner structure of (1) or (2) type can additionally reduce the decay width of cryptoexotic baryons and make it anomalously narrow (of the order of several tens of MeV). The theoretical predictions here are rather arbitrary. So the question of the existence of such narrow baryon resonances with hidden strangeness can be resolved only experimentally.

Thus, it seems quite desirable to perform the systematical search for cryptoexotic baryons B_ϕ with anomalous dynamical features which are listed below:

1. The dominant OZI allowed decay modes of B_ϕ baryons are the ones with strange particles in the final states (for ordinary baryons such decays have branching ratios at the percent level).
2. Cryptoexotic B_ϕ baryons can possess both a large mass ($\mathrm{M} > 1.8 \div 2.0\,\mathrm{GeV}$) and a narrow decay width ($\Gamma \leq 50 \div 100\,\mathrm{MeV}$). This is due to a complicated internal color structure of these baryons with significant quark rearrangement of color clusters in the decay processes and due to a limited phase space for the OZI allowed $B \to YK$ decays. At the same time typical decay widths of the well established $|qqq>$ isobars with similar masses are $\geq 300\,\mathrm{MeV}$.

As was emphasized in a number of papers [1,2,8,10,30,32,33], diffractive production processes with Pomeron exchange offer new tools in searches for the exotic hadrons. Originally, the interest was concentrated on the model of Pomeron with small cryptoexotic ($qq\bar{q}\bar{q}$) component [30,32]. In modern notions Pomeron is a multigluon system which allows for production of the exotic hadrons in gluon-rich diffractive processes (see Fig.1).

The Pomeron exchange mechanism in diffractive production reactions can induce the coherent processes on the target nucleus. In such processes the nucleus acts as a whole. Coherent processes can be easily identified by the transverse momentum spectra of the final state particle systems. They manifest themselves as diffractive peaks with large values of the slope parameters determined by the size of the nucleus: $\mathrm{d}N/\mathrm{d}P_\mathrm{T}^2 \simeq \exp(-bP_\mathrm{T}^2)$, where $b \simeq (8 \div 10)A^{2/3}\,\mathrm{GeV}^{-2}$. Owing to the difference in the absorption of single-particle and multiparticle objects in nuclei, coherent processes could serve as an effective tool for the separation of resonance against non-resonant multiparticle background (see, e.g. Ref.[34]). This idea is illustrated schematically in Fig.2.

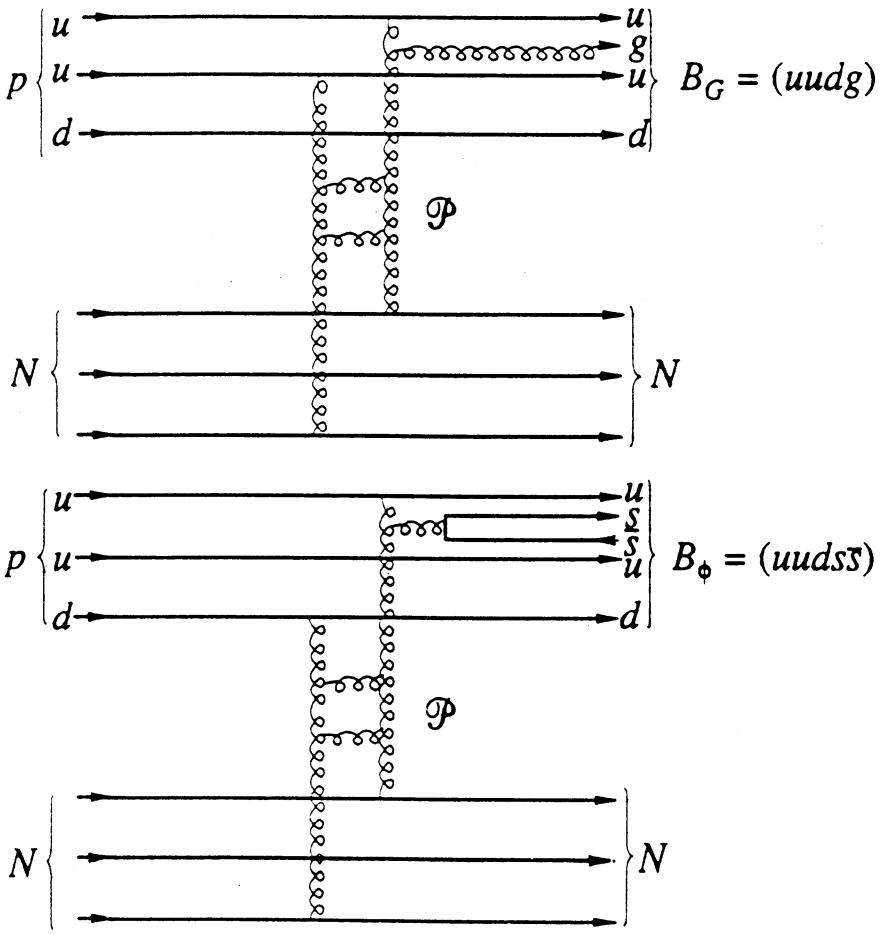

Fig. 1. The diagrams for exotic baryon production in the diffractive processes with Pomeron exchange (gluon-rich processes).

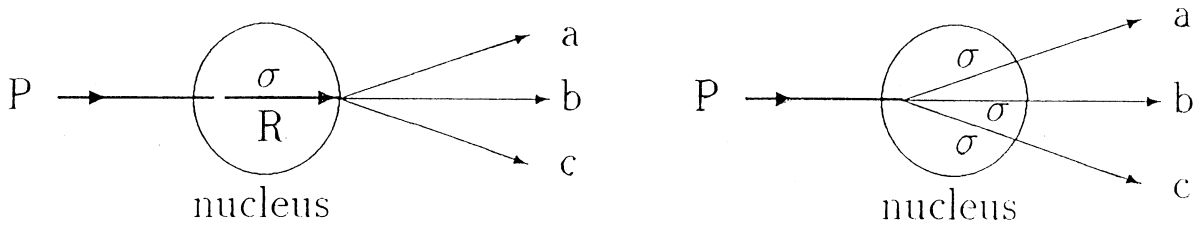

Fig. 2. Schematic illustration of the coherent suppression of non-resonance multiparticle background in the reactions p + (Nucleus) $\rightarrow R$ + (Nucleus), $R \rightarrow a + b + c$ (resonance production) and p + (Nucleus) $\rightarrow [abc]$ + (Nucleus) (nonresonant background) due to a difference in the resonance and background absorption in the target nuclei. As a result of this coherent suppression of nonresonant background it is possible to obtain: $\frac{\sigma_{\rm coh}({\rm resonance})}{\sigma_{\rm coh}({\rm background})} > \frac{\sigma_{\rm noncoh}({\rm resonance})}{\sigma_{\rm noncoh}({\rm background})}$.

3. The experiments with the SPHINX setup

A study of several proton-induced diffractive production processes

$$
\begin{aligned}
p + N &\rightarrow [pK^+K^-] + N && (5)\\
&\rightarrow [p\phi] + N, && (6)\\
&\quad\ \hookrightarrow K^+K^-\\
&\rightarrow [\Lambda(1520)K^+] + N, && (7)\\
&\quad\ \hookrightarrow K^-p,\\
&\rightarrow [\Sigma(1385)^0K^+] + N, && (8)\\
&\quad\ \hookrightarrow \Lambda\pi^0\\
&\rightarrow [\Sigma(1385)^0K^+] + N + (\text{neutrals}), && (9)\\
&\quad\ \hookrightarrow \Lambda\pi^0\\
&\rightarrow [\Sigma^0K^+] + N, && (10)\\
&\quad\ \hookrightarrow \Lambda\gamma\\
&\rightarrow [pp\bar{p}] + N, && (11)\\
&\rightarrow [p\omega] + N && (12)\\
&\quad\ \hookrightarrow \pi^+\pi^-\pi^0\\
&\rightarrow [p\pi^+\pi^-] + N, && (13)\\
&\rightarrow [\Delta^{++}\pi^-] + N. && (14)\\
&\quad\ \hookrightarrow p\pi^+
\end{aligned}
$$

and several other reactions was carried out by the SPHINX Collaboration in 70 GeV proton beam with a polyethylene target. The SPHINX detector used in these measurements includes a wide-aperture magnetic spectrometer with scintillator hodoscopes, proportional wire chambers, drift chambers and a multichannel γ-spectrometer made of total absorption lead glass detectors. Charged particles of the final state were identified with differential RICH spectrometer and two multicell gas threshold Cherenkov counters $\breve{C}_1$ and $\breve{C}_2$. The layout of the SPHINX setup is presented on Fig.3. A detailed description of the apparatus can be found in Ref.[12].

For the separation of different exclusive reactions a complete kinematic reconstruction of the events was used with the account of the information from tracking detectors, magnetic spectrometer, γ - spectrometer and all Cherenkov counters of the SPHINX setup. In the final stage of this reconstruction procedure the identification of the reactions under study was achieved by the examination of effective mass spectra for subsystems of secondary particles, as it is illustrated in Fig.4.

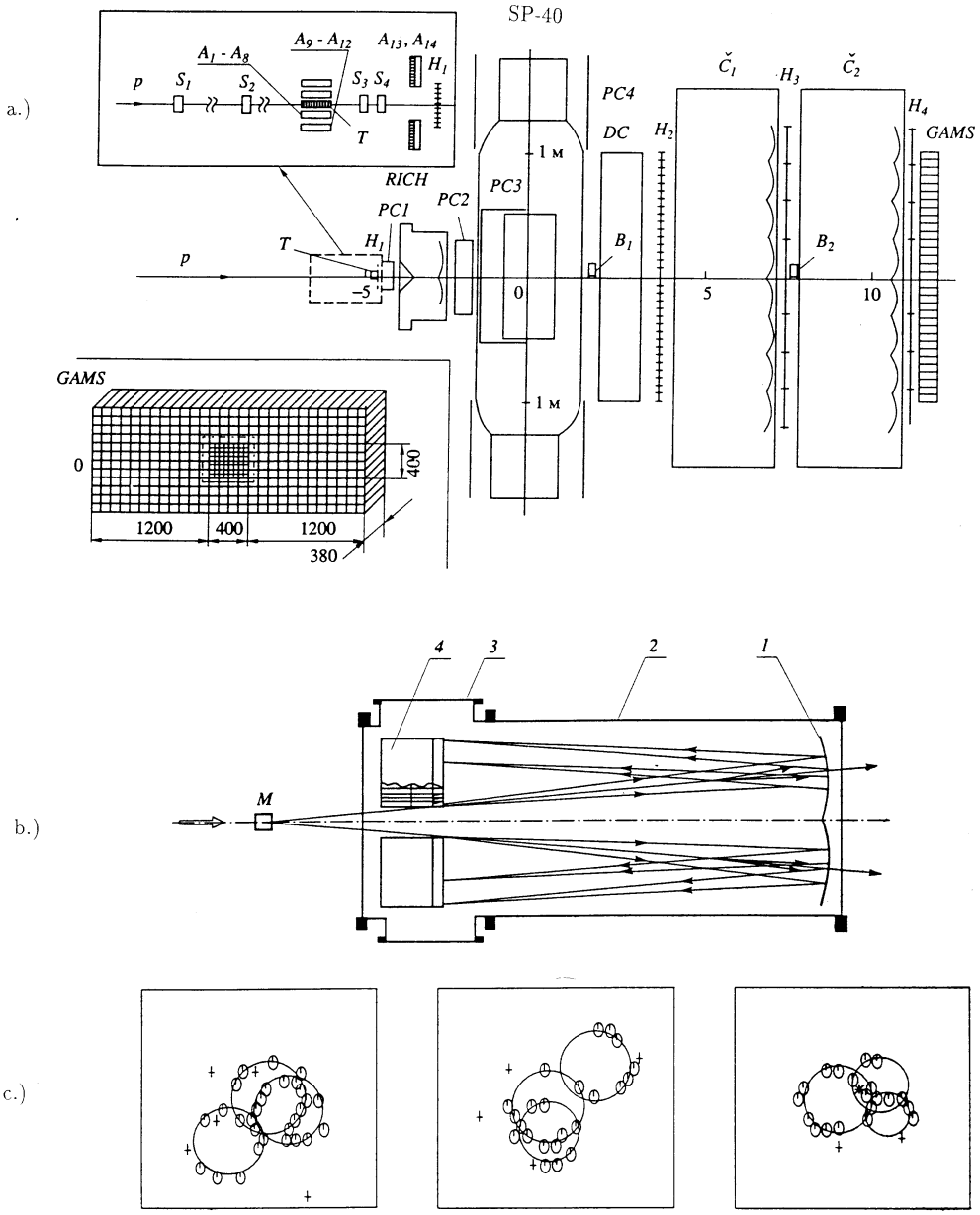

Fig. 3. a) The layout of the SPHINX spectrometer. $S1-S4$, $B1$, $B2$ are scintillation counters, $A1-A14$ are scintillation guard counters, $H1-H4$ are scintillation hodoscopes; $PC1-PC4$ are blocks of proportional chambers; DC is the block of drift chambers; SP - 40 is a spectrometer magnet; $\check{C}_1, \check{C}_2$ are hodoscope threshold Cherenkov counters; RICH is a Cherenkov ring image spectrometer; GAMS is the hodoscope γ - spectrometer (which is presented on the left lower part of the figure; the dutt-dotted line indicates the active region of γ detector which is used for trigger requirement). b) The layout of Cherenkov RICH spectrometer with registration of the radiation rings: 1) - spherical mirror from the thin glass ($\Delta = 5\,\text{mm}$, $f = 1250\,\text{mm}$); 2) - the body of the counter; 3) - flanges; 4) - photomatrix with 736 phototubes FEU-60 with the photocathode 10 mm in diameter. c) The examples of the registrating Cherenkov radiation rings in photomatrix of the RICH spectrometer for the trigger events with 3 charged particles in the final state.

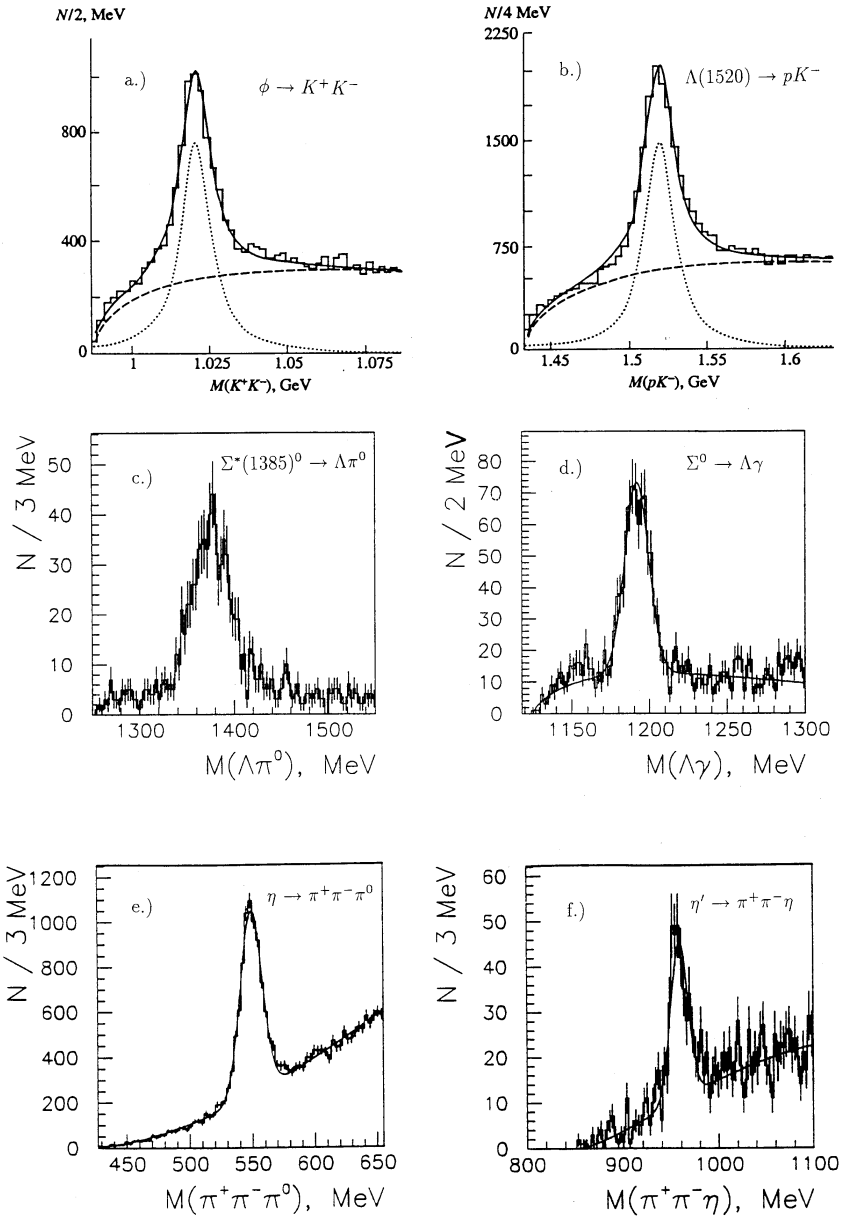

Fig. 4. a, b) Selection of the reactions $p + N \to [p\phi] + N$ and $p + N \to [\Lambda(1520)K^+] + N$ from the invariant mass spectra $M(K^+K^-)$ and $M(pK^-)$ produced in the reaction $p + N \to [pK^+K^-] + N$.
c) Selection of the reaction $p + N \to [\Sigma^*(1385)^0K^+] + N$ from the invariant mass spectrum $\Lambda\pi^0$ produced in the reaction $p + N \to [\Lambda\pi^0K^+] + N$.
d) Selection of the reaction $p + N \to [\Sigma^0K^+] + N$ from the invariant mass spectrum of $(\Lambda\gamma)$ produced in the reaction $p + N \to [\Lambda\gamma K^+] + N$.
e) Selection of the reactions $p + N \to [p\eta] + N$ from the invariant mass spectrum $M(\pi^+\pi^-\pi^0)$ in $p + N \to [p\pi^+\pi^-\pi^0] + N$
f) Selection of the reaction $p + N \to [p\eta'] + N$ from the invariant mass spectrum $M(\pi^+\pi^-\eta)$ in $p + N \to [p\pi^+\pi^-\eta] + N$.

As is seen from dN/dP_T^2 spectra for above mentioned processes, there are strong narrow forward cones in these distributions with the slope $b \geq 40 - 50$ GeV^{-2} which correspond to a coherent diffractive production on carbon nuclei (Fig.5). For identification of the coherently produced events "loose" or "tight" cuts in P_T^2 can be used:

1. "loose" transverse momentum cut:$P_T^2 < 0.075 \div 0.1$ GeV^2; with this cut noncoherent background in event sample can be as large as 30-40%;
2. "tight" transverse momentum cut: $P_T^2 < 0.02$ GeV^2; with this cut noncoherent background is reduced to $< 8 - 10\%$ of the event sample at the cost of lower signal statistics.

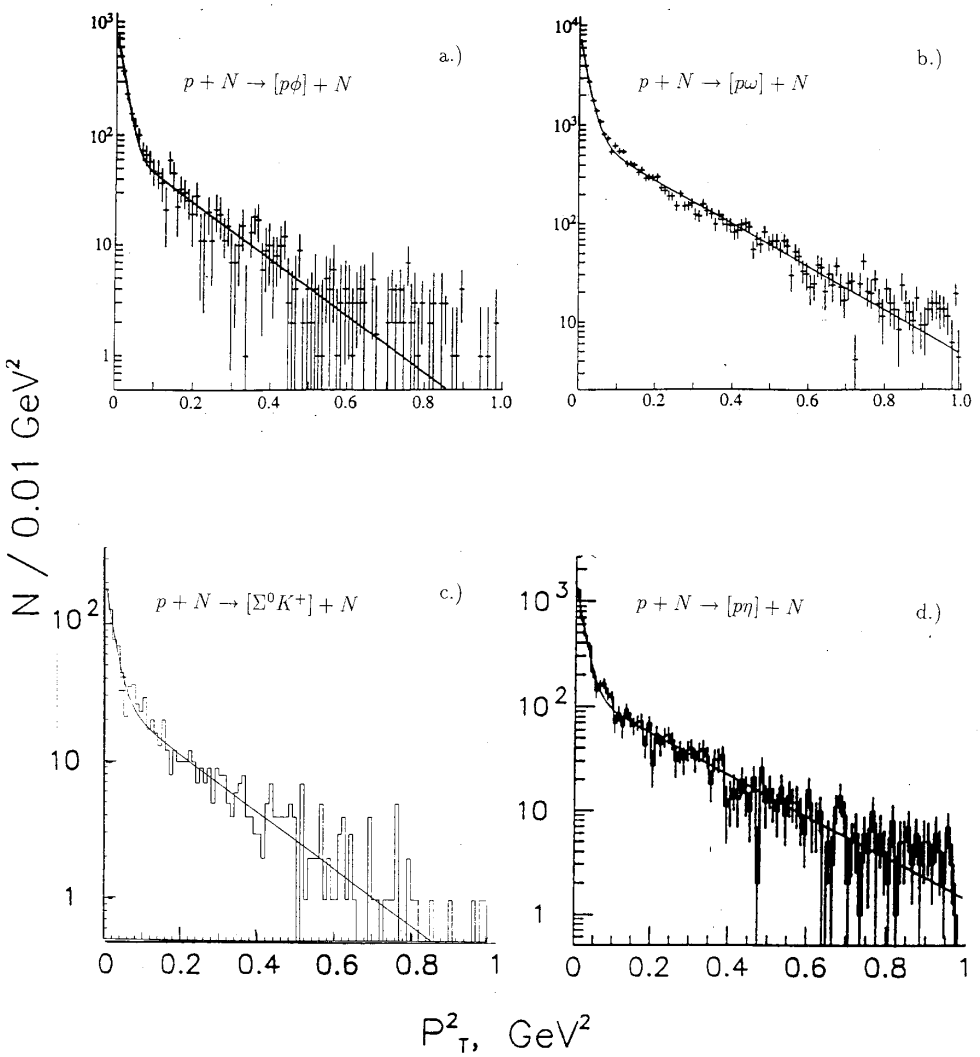

Fig. 5. dN/dP_T^2 distributions for several reactions: a) for the reaction $p + N \to [p\phi] + N$; b) for the reaction $p + N \to [p\omega] + N$; c) for the reaction $p + N \to [\Sigma^0 K^+] + N$; d) for the reaction $p + N \to [p\eta] + N$. In all these distributions there are strong narrow forward cones with the slope $b \geq 40 - 50$ GeV^{-2}, which correspond to coherent diffractive production processes on carbon nuclei.

All diffractive and coherent reactions mentioned above were used for thorough searches for new baryon states, especially for candidates for cryptoexotic baryons with hidden strangeness [12-21]. But the most interesting results were obtained in a study of $\Sigma^*(1385)^0K^+$ and Σ^0K^+ systems produced in the coherent diffractive reactions on carbon nuclei

$$\begin{array}{rcl} p+C & \rightarrow & [\Sigma(1385)^0K^+]+C \\ & & \hookrightarrow \Lambda\pi^0 \\ & & \hookrightarrow p\pi^- \end{array} \qquad (15)$$

and

$$\begin{array}{rcl} p+C & \rightarrow & [\Sigma^0K^+]+C. \\ & & \hookrightarrow \Lambda\gamma \\ & & \hookrightarrow p\pi^- \end{array} \qquad (16)$$

4. Previous data on the coherent diffractive reactions $p+C \rightarrow [\Sigma(1385)^0K^+]+C$ and $p+C \rightarrow [\Sigma^0K^+]+C$ [18-20]

4.1. Reaction $p+C \rightarrow [\Sigma(1385)^0K^+]+C$

In the analysis of the SPHINX data the exclusive process with Λ hyperons $p+N \rightarrow [\Lambda\pi^0K^+]+N$ was identified [13,14]. In Fig.4c the invariant mass spectrum of the $\Lambda\pi^0$ system in this reaction is presented. In the $M(\Lambda\pi^0)$ spectrum a peak corresponding to the $\Sigma(1385)^0 \rightarrow \Lambda\pi^0$ decay is dominating. The background level under the $\Sigma(1385)^0$ peak is quite small. This fact simplifies the identification of reaction $p+N \rightarrow [\Sigma(1385)^0K^+]+N$ and corresponding coherent reaction (15).

Coherent events of (15) were singled out in the analysis of dN/dP_T^2 distribution as a strong forward peak with the slope $b \sim 50$ GeV^{-2}. In order to reduce the noncoherent background and to obtain the $\Sigma(1385)^0K^+$ mass spectrum for the "pure" coherent production reaction on carbon nuclei a "tight" requirement $P_T^2 < 0.02$ GeV^2 has been imposed and the mass spectra of $\Sigma(1385)^0K^+$ for the coherent events of (15) have been obtained (see, for example, Fig.6). These spectra were studied with different values of ΔM bin widths in histograms and with bin shifting. The thorough background evaluation under the peaks was obtained using the information on the side bands near the peak. The statistical confidence levels of the peaks were determined from these data. See more details in [19].

The fits of the spectra with Breit-Wigner peaks and polynomial smooth background were carried out, and the average values for the main parameters of $X(2050)$ structure were determined:

$$\left.\begin{array}{l} M = 2052 \pm 6\,\text{MeV}; \\ \Gamma = 35^{+22}_{-35}\text{MeV} \\ \text{(with the account of the apparatus mass resolution);} \\ \text{statistical C.L. of the peak } \geq \text{ 5 standard deviations .} \end{array}\right\} \qquad (17)$$

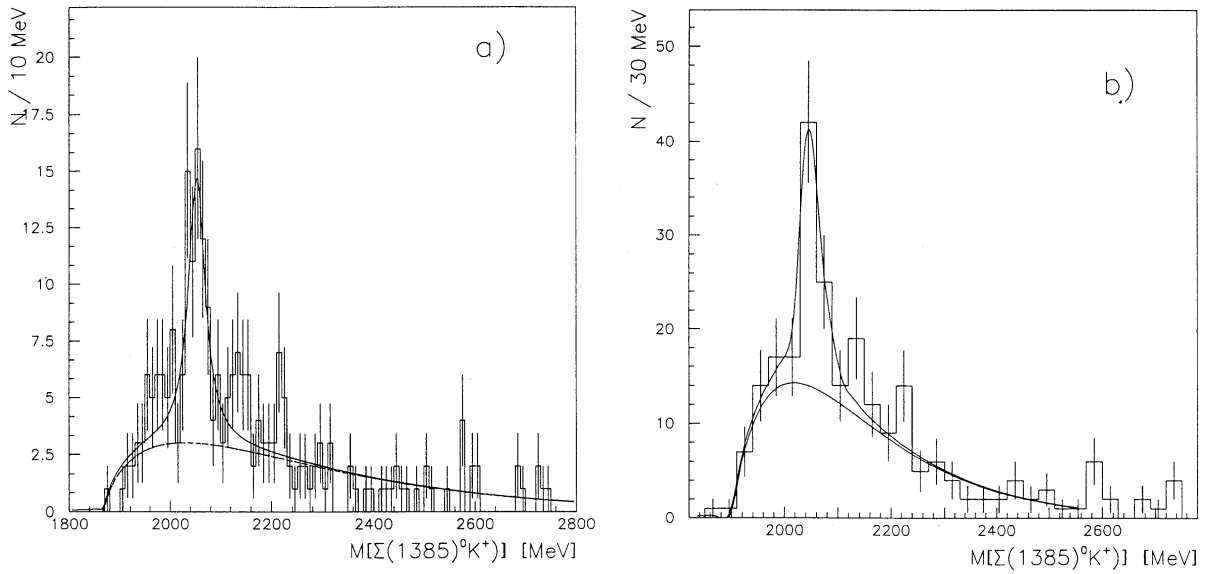

Fig. 6. The invariant mass spectra $M[\Sigma^0(1385)K^+]$ in the coherent reaction (15) with tight transverse momentum cut $P_T^2 < 0.02$ GeV^2 and with different widths of bins: a) $\Delta M =$ 10 MeV; b) $\Delta M = 30$ MeV. The spectra are fitted by the sum of smooth polynominal background curve and $X(2050)$ peak. The parameters of $X(2050)$ peak are: a) $M =$ 2053 ± 4 MeV, $\Gamma = 40 \pm 15$ MeV; b) $M = 2053 \pm 5$ MeV, $\Gamma = 35 \pm 16$ MeV.

This narrow structure cannot be explained by diffractive nonresonant process of the Deck-type and seems to be caused by the production of a new cryptoexotic baryon with hidden strangeness.

The reaction $n + N \to \Sigma(1385)^- K^+ + ...$ with limited multiplicity of charged particles in the final state (we refer to it as "a reaction with limited inclusiveness") was studied earlier in experiments with the BIS-2 detector in the neutron beam of the IHEP accelerator at the mean energy $< E_n > \simeq 40$ GeV of incident neutrons [10]. A narrow structure with mass $M = 1956^{+8}_{-6}$ MeV and anomalously small width $\Gamma = 27 \pm 15$ MeV was observed in the effective mass spectrum of the $\Sigma(1385)^- K^+$ system and interpreted as a candidate for the cryptoexotic baryon $N_\phi = |uddss\bar{s} >$ with hidden strangeness. This structure was called the $N_\phi(1960)$ baryon [10]. The BIS-2 results on the cross section of $N_\phi(1960)$ production are presented in Table 1.

In the experiments with the SPHINX spectrometer the search for $N_\phi(1960)$ production was performed in exclusive "elastic" reaction (8) and in partially inclusive reaction (9).

Analysis of the $M[\Sigma(1385)^0 K^+]$ spectra in these reactions in various transverse-momentum intervals did not reveal any structures corresponding to $N_\phi(1960)$ baryon production in either the overall mass spectra (plotted for all P_T^2 values) or in the spectra for coherent processes, that is, for $P_T^2 < 0.075$ GeV^2.

Upper limits on the cross sections for $N_\phi(1960)$ production, which were obtained in the SPHINX experiment are presented in Table 1. These upper limits are significantly lower than the value of the cross section for $N_\phi(1960)$ production that was obtained in the BIS-2 experiment. Strictly speaking, there is no direct contradiction between the BIS-2

and SPHINX results because they apply to somewhat different prosesses[1]. However, the large disparity between the two cross-section estimates (see Table 1), as well as very hard background conditions for $\Sigma^*(1385)^+$ and $N_\phi(1960)^0$ separation in BIS-2 measurements cast some doubts on the real existence of $N_\phi(1960)$ baryon (for a more detailed discussion, see Refs. [13-16]).

Table 1. Estimates of cross sections for N_ϕ baryon production

The BIS-2 data [10]	The SPHINX data (upper limits on the cross sections at the 95% confidence level) [13-16]	
Reaction with limited inclusiveness $n + N \longrightarrow N_\phi(1960) + \ldots$	"Elastic" reaction $p + N \longrightarrow N_\phi(1960) + N$	Partially inclusive reaction $p + N \longrightarrow N_\phi(1960) + N$ + (neutrals)
$\sigma[N_\phi(1960)]\|_C \cdot BR$	Coherent process ($P_T^2 < 0.075$ GeV^2)	
$= \begin{cases} 1725 \pm 285 \text{ nb/(C nucleus)}, \\ \text{or with allowance for the factor 1.7} \\ \sim 3 \times 10^3 \text{ nb/(C nucleus)} \end{cases}$	$\sigma[N_\phi(1960)]\|_C \cdot BR < 660$ nb/(C nucleus) $\sigma[N_\phi(1960)]\|_{nucleon} \cdot BR$ $< \begin{cases} 55 \text{ nb/nucleon } (\sigma \sim A) \\ 125 \text{ nb/nucleon } (\sigma \sim A^{2/3}) \end{cases}$	$\sigma[N_\phi(1960)]\|_C \cdot BR < 820$ nb/(C nucleus) $\sigma[N_\phi(1960)]\|_{nucleon} \cdot BR$ $< \begin{cases} 70 \text{ nb/nucleon } (\sigma \sim A) \\ 150 \text{ nb/nucleon } (\sigma \sim A^{2/3}) \end{cases}$
$\sigma[N_\phi(1960)]\|_{nucleon} \cdot BR$	For all P_T^2 values	
$= \begin{cases} 330 \pm 60 \text{ nb/nucleon}, \\ \text{or with allowance for the factor 1.7} \\ \sim 550 \text{ nb/nucleon} \end{cases}$ for $\sigma \sim A^{2/3}$	$\sigma[N_\phi(1960)]\|_{nucleon} \cdot BR < 120$ nb/nucleon	$\sigma[N_\phi(1960)]\|_{nucleon} \cdot BR < 230$ nb/nucleon

Note: Here, $\sigma[N_\phi(1960)]|_C$ is the cross section of the corresponding reaction per carbon nucleus; $\sigma[N_\phi(1960)]|_{nucleon}$ is the cross section of the same reaction per nucleon; $\sigma \sim A$ (this is possible for the coherent reactions); $BR = BR[N_\phi(1960) \longrightarrow \Sigma(1385)K]$ for all isospin states. It should be borne in mind that the determination of cross sections in the BIS-2 experiment was not quite correct. Applying the fitting procedure used in the analysis of the SPHINX data to the BIS-2 data, we find that the number of events in the N_ϕ peak and the corresponding cross section value should be multiplied by a factor of 1.7 - 2.0.

4.2. Reaction $p + C \to [\Sigma^0 K^+] + C$

During the study of the reactions with Λ hyperons and K mesons the events with one and only one additional γ-cluster detected in γ-spectrometer of the SPHINX apparatus were separated.

Invariant mass spectrum of the $\Lambda\gamma$ system for these events is shown in Fig.4d. A peak corresponding to the $\Sigma^0 \to \Lambda\gamma$ decay is clearly seen in this spectrum, allowing for identification of reaction (16). Coherent events were selected using a P_T^2 cut.

Invariant mass spectrum $M(\Sigma^0 K^+)$ in the coherent reaction (16) for $P_T^2 < 0.1\text{GeV}^2$ is shown in Fig.7. Apart from a small bump with $M \sim 1800$ MeV at the threshold, $X(2000)$-peak dominates the spectrum. The following parameters were measured for this peak:

$$\left.\begin{array}{l} M = 1997 \pm 7\,\text{MeV}; \\ \Gamma = 91 \pm 17\,\text{MeV}; \\ \text{statistical significance of the peak is 7 s.d.} \end{array}\right\} \qquad (18)$$

[1]The only unequivocal conclusion that can be drawn is that the statement concerning the diffractive nature of $N_\phi(1960)$ production in the BIS-2 experiment [10] is in contradiction with their own data on the P_T^2 distribution of the events and with the SPHINX results. Thus, this statement is incorrect.

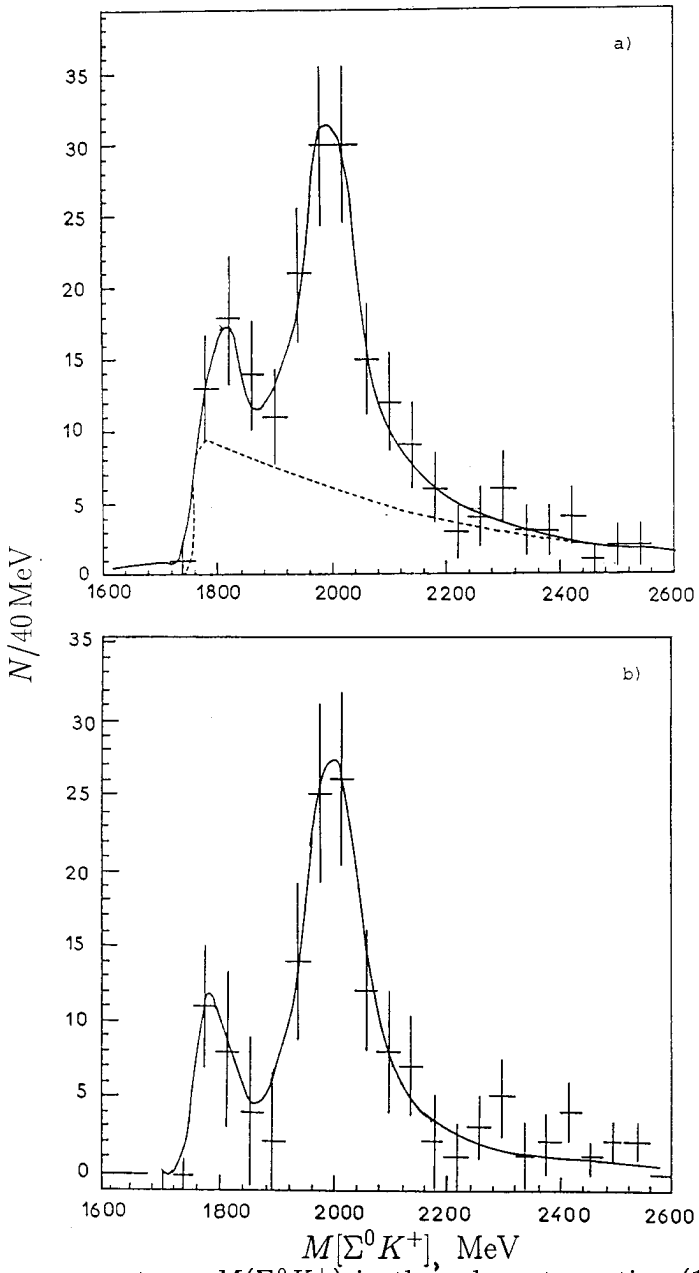

Fig. 7. Invariant mass spectrum $M(\Sigma^0 K^+)$ in the coherent reaction (16) ($P_T^2 < 0.1$ GeV^2): a) - for all the events in the Σ^0 signal band in Fig.4d; b) - after sideband subtraction of the background under Σ^0 - peak in Fig. 4d (old SPHINX data, see Ref. [19] for details).

Such a shape of the $\Sigma^0 K^+$ mass spectrum (with an additional structure at the threshold) proves that the $X(2000)$ peak cannot be explained by a non-resonant Deck-type diffractive singularity. Therefore, this peak possibly has a resonant nature.

4.3. Study of other decay channels for $X(2050)$ and $X(2000)$ states

A search for other decay channels of the $X(2000)$ and $X(2050)$ baryon candidates was performed by analyzing data produced in the coherent reactions

$$p + C \rightarrow [p\pi^+\pi^-] + C \quad (19)$$

$$\rightarrow [\Delta(1232)^{++}\pi^-] + C. \quad (20)$$

These data were also collected by the SPHINX detector in kinematic conditions similar with (15) and (16). A preliminary analysis of the reaction with $\Delta(1232)^{++}\pi^-$ production was a subject of our earlier paper [13]. In this paper a diffractive production of two isobar-like structures with masses ≈ 1460 MeV and ≈ 1715 MeV was observed in the data. However, no peaks in 2 GeV mass range were observed in the mass spectra of $p\pi^+\pi^-$ and $\Delta(1232)^{++}\pi^-$ systems produced in reactions (19) and (20), respectively. Lower limits on the corresponding decay branching ratios were set to be (at the 95% C.L.):

$$\mathrm{R}_1 = \frac{\mathrm{BR}\{X(2050)^+ \rightarrow [\Sigma(1385)K]^+\}}{\mathrm{BR}\{X(2050)^+ \rightarrow [\Delta(1232)\pi]^+\}} > 1.7 \quad (21)$$

$$\mathrm{R}_2 = \frac{\mathrm{BR}\{X(2050)^+ \rightarrow [\Sigma(1385)K]^+\}}{\mathrm{BR}\{X(2050)^+ \rightarrow p\pi^+\pi^-\}} > 2.6 \quad (22)$$

$$\mathrm{R}'_2 = \frac{\mathrm{BR}\{X(2050)^+ \rightarrow \Sigma(1385)^0K^+\}}{\mathrm{BR}\{X(2050)^+ \rightarrow p\pi^+\pi^-\}} > 0.86 \quad (23)$$

$$\mathrm{R}_3 = \frac{\mathrm{BR}\{X(2000)^+ \rightarrow [\Sigma K]^+\}}{\mathrm{BR}\{X(2000)^+ \rightarrow [\Delta(1232)\pi]^+\}} > 0.83 \quad (24)$$

$$\mathrm{R}_4 = \frac{\mathrm{BR}\{X(2000)^+ \rightarrow [\Sigma K]^+\}}{\mathrm{BR}\{X(2000)^+ \rightarrow p\pi^+\pi^-\}} > 7.8 \quad (25)$$

$$\mathrm{R}'_4 = \frac{\mathrm{BR}\{X(2000)^+ \rightarrow \Sigma^0K^+\}}{\mathrm{BR}\{X(2000)^+ \rightarrow p\pi^+\pi^-\}} > 2.6 \quad (26)$$

Isotopic relations between the decay amplitudes of $I = \frac{1}{2}$ particles were assumed in these calculations ($X(2000)$ and $X(2050)$ states belong to isodoublets since they are produced in a diffractive dissociation of a proton).

Ratios $R_1 - R_4$ of the widths of the $X(2000)$ and $X(2050)$ decays into strange and nonstrange particles are much larger than those for ordinary (qqq)- isobars [2,18].

Narrow widths of the $X(2000)$ and $X(2050)$ baryon states as well as anomalously large branching ratios for their decay channels with strange particles emission (large values of $R_1 - R_4$) are the reasons to consider these states as serious candidates for cryptoexotic baryons with a hidden strangeness ($|uuds\bar{s}>$). At the existing level of statistics for reactions (15) and (16), as well as with possible background uncertainties the above results and conclusions must be considered as preliminary. They should be confirmed in further measurements with greatly increased statistics.

The problem of possible connection between the $X(2050)$ baryon state observed in reaction (15) and the $X(2000)$ baryon state observed in reaction (16) seems to be quite interesting. At a first sight the difference in their parameters (17) and (18) is significant one. But to obtain the ultimate answer on the existence of two different baryonic states or only one state with two different decay channels we need to perform a further study of reactions (15) and (16) with increased statistics. It would give a possibility to obtain

more precise information about the shape of these peaks, their decay widths and quantum numbers and to clear out a possible connection between these two structures.

Some new data on reaction (16) obtained with a partially upgraded SPHINX setup will be discussed below.

5. SPHINX detector upgrade

The SPHINX detector is undergoing a complete upgrade. It includes a new tracking system with proportional wire chambers and drift tubes, a new γ-spectrometer, new electronics, trigger systems, DAQ, and on-line computers. When this modernization will be finished, the SPHINX apparatus will have a possibility to work with higher luminosity and with significantly increased number of recorded triggers per accelerator burst (2-3 thousand versus 3-hundred events per burst, collected with the existing DAQ).

At the first stage of the upgrade program we made several refinements:

1. A new γ-spectrometer with 39×27=1052 lead glass counters with the 5 cm $\times$ 5 cm $\times$ 42 cm dimensions was installed in the setup instead of the old γ-spectrometer [12] (with 320 lead glass counters with the 10 cm $\times$ 10 cm $\times$ 38 cm dimensions and only 63 counters of the 5 cm $\times$ 5 cm $\times$ 38 cm size in the central part of the photon detector). A new γ-spectrometer is a modified version of the IHEP IGD γ-spectrometer which was used previously in the EGS experiment at CERN .
2. Four additional planes of the drift tubes were installed between the multicell threshold Cherenkov counter and the γ-spectrometer (see layout of the SPHINX apparatus, Fig.3). In a modernized setup we removed the threshold Cherenkov counter $\breve{C}_2$ because of a good identification capability of the RICH and $\breve{C}_1$ Cherenkov detector based system.
3. New trigger requirements made it possible to detect $\Lambda \to p\pi^-$ decays on the $L \approx$ 300 cm decay path (instead of $L \approx 30$ cm in the previous runs).

As a result of this upgrade a detection efficiency and purity of the Λ events were significantly increased. Better photon identification in the new γ-spectrometer allows to reduce backgrounds due to hadron showers and lost photons. This is particularly important for identification of single photons (e.g., in the radiative $\Sigma^0 \to \Lambda\gamma$ decays). To illustrate these new features we present $\Lambda \to p\pi^-$ peak observed in the old and new $p + N \to \Lambda K^+ + N$, $\Lambda \to p\pi^-$ data (Figs.8,9), as well as the identification of Σ^0 in the $p + N \to \Sigma^0 K^+ + N$, $\Sigma^0 \to \Lambda\gamma$ reaction (Figs. 4d, 10). It is clear that with a partially upgraded SPHINX detector we can select reactions with Λ and Σ^0 hyperons production much more effectively.

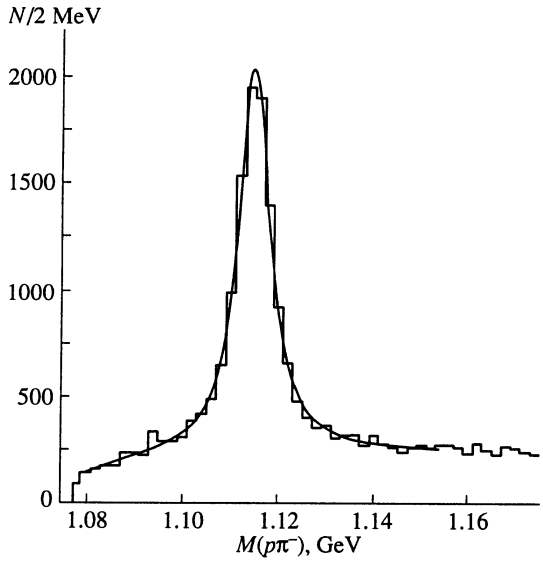

Fig. 8. Selection of the reaction $p + N \to [\Lambda K^+] + N$ from the invariant mass spectrum of $(p\pi^-)$ produced in the reaction $p+N \to [p\pi^- K^+]+N$ (data were collected with an old version of the SPHINX detector with the $\Lambda \to p\pi^-$ decay path $L \simeq 30$ cm; it was impossible to resolve effectively the primary and secondary vertices).

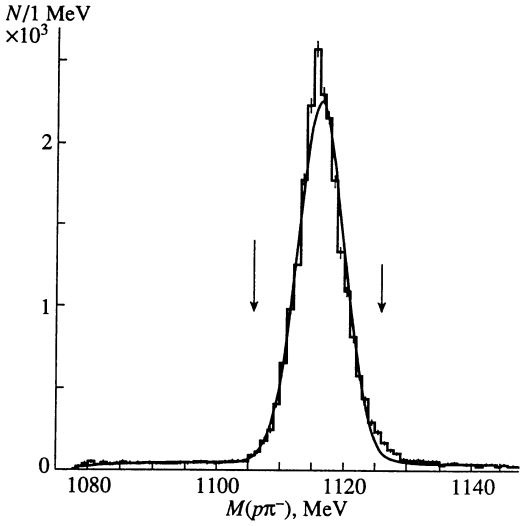

Fig. 9. Selection of the reaction $p + N \to [\Lambda K^+] + N$ from the exclusive $p + N \to [p\pi^- K^+] + N$ data taken with the upgraded SPHINX detector with the $\Lambda \to p\pi^-$ decay path $L \approx 300$ cm which allowed for a reliable identification of Λ decay vertices. Background under Λ peak in the $M(p\pi^-)$ spectrum is significantly reduced comparing to that in Fig.8.

6. New $p + C \to [\Sigma^0 K^+] + C$ data from a special run with the partially upgraded SPHINX spectrometer [21]

The production of the $(\Sigma^0 K^+)$ system in the $p+N \to [\Lambda\gamma K^+]+N$ reaction was clearly identified (see Fig.10) with the partially upgraded SPHINX spectrometer in a special test run. Background under the Σ^0 peak is small, which simplifies selection of the reactions under study since there is no need for background subtraction in this case. To select a coherent reaction (16) we used the "loose" cut on the transverse momentum $P_T^2 < 0.1$ GeV^2, as it was done in the previous analysis. The invariant mass spectrum $M(\Sigma^0 K^+)$ for this coherent reaction from new data is presented in Fig.11. This spectrum is in a good agreement with that in Fig.7: there is again a clear $X(2000)$ peak and a threshold structure with $M \sim 1800$ MeV. The combined spectrum from the old data (Fig.7b) and new data (Fig.11) is presented in Fig.12. A sum of the spectra in Fig.7a (no background subtraction) and Fig.11 gives a similar result. The average parameters of the $X(2000)$ structure obtained from the different combined $M(\Sigma^0 K^+)$ invariant mass spectra are:

$$\left.\begin{array}{l} M = 1996 \pm 7\,\text{MeV}; \\ \Gamma = 99 \pm 21\,\text{MeV}; \\ \text{statistical significance of the peak} > 10\ \text{s.d.} \end{array}\right\} \qquad (27)$$

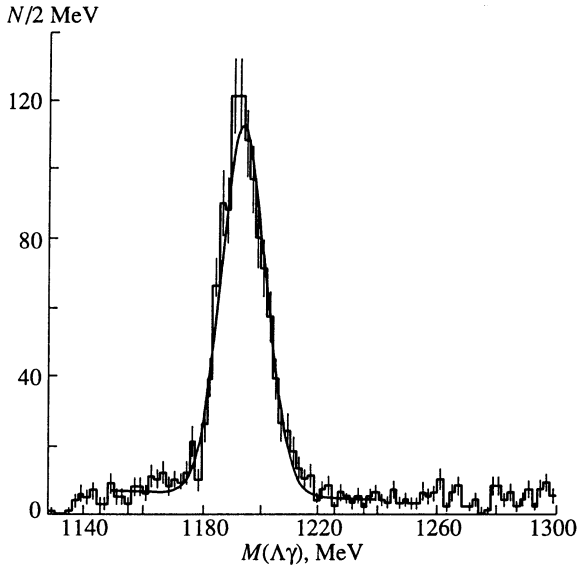

Fig. 10. Selection of the reaction $p + N \rightarrow [\Sigma^0 K^+] + N$ from the invariant mass spectrum of the $(\Lambda\gamma)$ system produced in the reaction $p + N \rightarrow \Lambda\gamma K^+ + N$. Data were taken with the upgraded SPHINX detector with an improved identification of $\Lambda \rightarrow p\pi^-$ decay and single photon in the new γ-spectrometer. Background under Σ^0 peak in $M(\Lambda\gamma)$ is significantly reduced compared to that in Fig.4d.

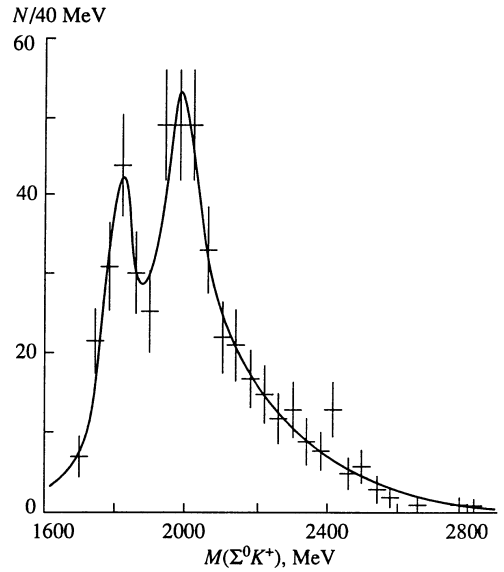

Fig. 11. Invariant mass spectrum of the $(\Sigma^0 K^+)$ system produced in the coherent reaction (16) in a special run of the upgraded SPHINX detector ($P_T^2 < 0.1$ GeV^2). Because of the low background under Σ^0-peak in Fig.10 no background subtraction was done in the $M(\Sigma^0 K^+)$ spectrum. The results on the $(\Sigma^0 K^+)$ mass spectrum from this run are in a good agreement with the old data [18, 19, 20], see Fig.7.

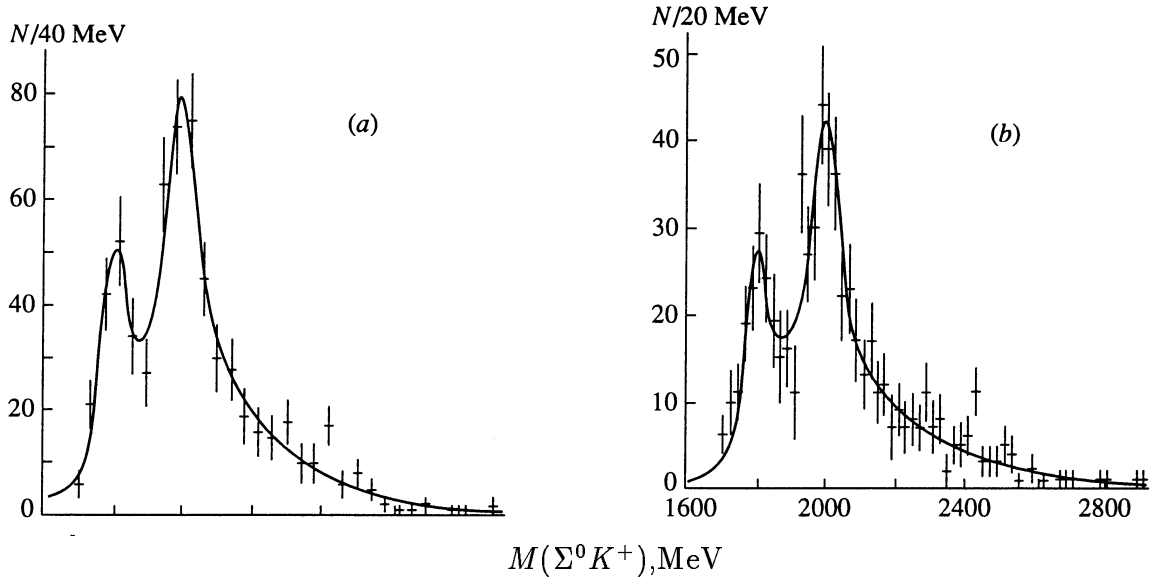

Fig. 12. Combined mass spectrum $M(\Sigma^0 K^+)$ for the data in Figs.7b and 11: a) 40 MeV mass bin; parameters of the $X(2000)$ peak are $M = 1995 \pm 7$ MeV and $\Gamma = 103 \pm 19$ MeV; b) 20 MeV mass bin; parameters of the $X(2000)$ peak are $M = 2001 \pm 7$ MeV and $\Gamma = 88 \pm 25$ MeV.

It is important to mention that the old and new data from the coherent diffractive reaction (16) were obtained under different experimental conditions, with significant modifications in the detector, different background and systematics. Nevertheless, the $\Sigma^0 K^+$ invariant mass spectra from two runs are in a good agreement which makes them more reliable.

An increased statistics allowed for a detailed study of the effect of a "tight" P_T^2 cut on the shape of the $\Sigma^0 K^+$ mass spectrum. The tight cut reduces a noncoherent background and therefore enhances the coherent process (16). As was shown before [18, 19] the parameters of the $X(2000)$ peak are not affected by the tight P_T^2 cut. However, we quite unexpectedly found a strong influence of this cut on the shape of the threshold structure at 1800 MeV. As is seen from Fig.13, this structure is produced only at very small P_T^2. For $P_T^2 < 0.01$ GeV^2 it is clearly observed and has the parameters

$$\left.\begin{array}{l} M = 1812 \pm 7\,\text{MeV}; \\ \Gamma = 56 \pm 16\,\text{MeV}. \end{array}\right\} \qquad (28)$$

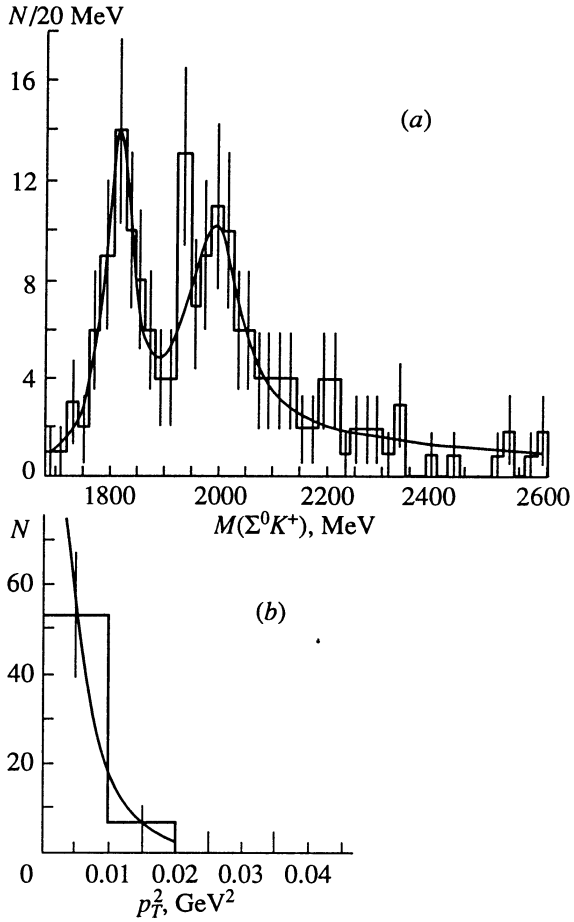

Fig. 13. Study of a narrow threshold structure in the mass spectrum of the $(\Sigma^0 K^+)$ system produced in the coherent reaction (16) (data taken with the upgraded SPHINX setup): a) invariant mass spectrum $M(\Sigma^0 K^+)$ for $P_T^2 < 0.01$ GeV^2; a threshold structure with $M = 1812 \pm 7$ MeV and $\Gamma = 56 \pm 16$ MeV is clearly seen; b) a P_T^2 dependence for this threshold structure production.

These peculiar properties of the threshold structure are not well understood yet and require a further study with larger statistics and under different experimental conditions (e.g. in the coherent processes with heavier nuclei).

It is possible to modify P_T cut for the events of coherent reaction (16) to suppress the influence of the threshold structure and to observe the $X(2000)$ peak in more clear conditions.

This new transverse momentum cut is: $0.01 < P_T^2 < 0.1$ GeV^2. The corresponding results in combined $\Sigma^0 K^+$ invariant mass spectrum are presented on Fig.14 (to be compared with Fig.12 for $P_T^2 < 0.1$ GeV^2).

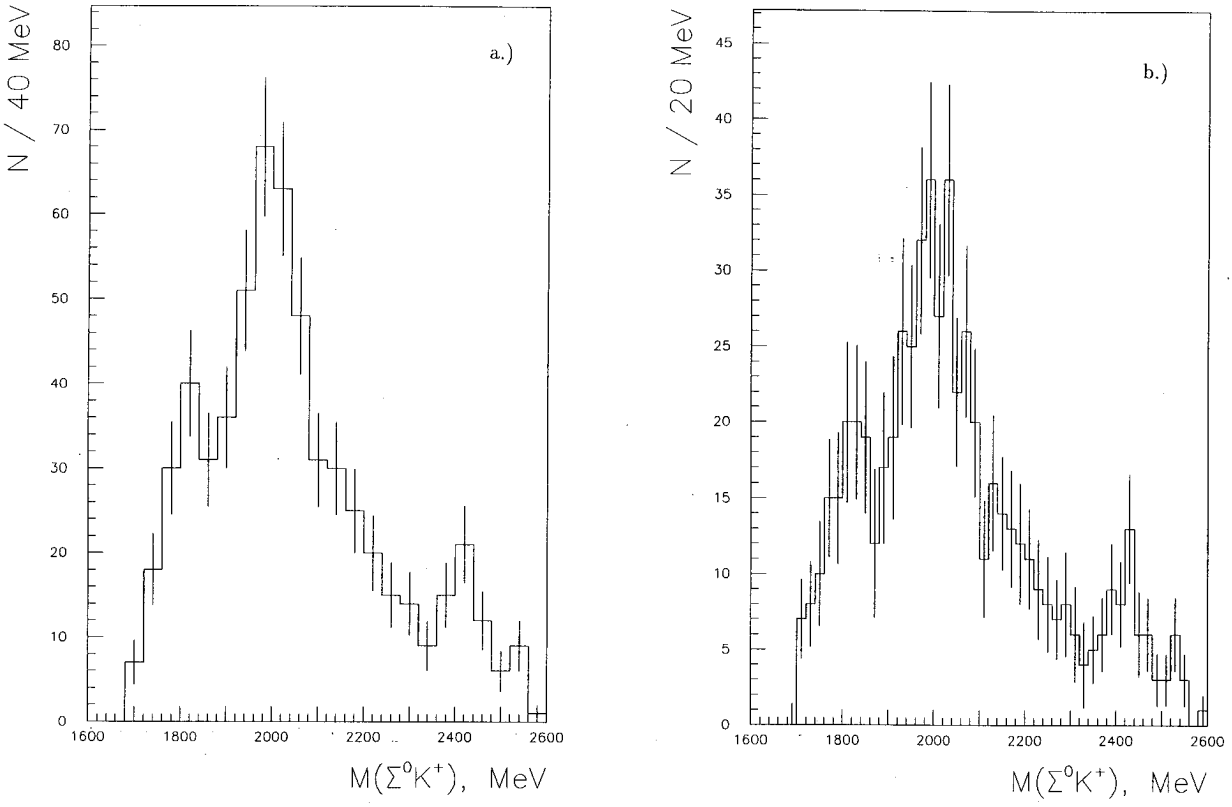

Fig. 14. a,b) The same $M(\Sigma^0 K^+)$ combined mass spectra as on Fig. 12 a,b, but with modified coherent cut $0.01 < P_T^2 < 0.1$ GeV^2 (to reduce the influence of the threshold structure of Fig.13).

7. Reactions $p + N \to [p\eta] + N$ and $p + N \to [p\eta'] + N$ [20]

In the study of exclusive diffractive-like reactions with $\pi^+\pi^-$ pairs and two photon clusters in the final state ($p + N \to [p\pi^+\pi^-\gamma\gamma] + N$) clear peaks of π^0 and η are seen in the effective mass spectrum of $\gamma\gamma$ pairs, and the reactions

$$p + N \rightarrow [p\pi^+\pi^-\pi^0] + N, \quad (29)$$
$$\hookrightarrow \gamma\gamma$$
$$\rightarrow [p\pi^-\pi^-\eta] + N, \quad (30)$$
$$\hookrightarrow \gamma\gamma$$

are well separated. The first reaction is used to study $[p\eta]$ and $[p\omega]$ production processes. As is seen from Fig.4e, the reaction

$$p + N \rightarrow [p\eta] + N, \quad (31)$$
$$\hookrightarrow \pi^+\pi^-\pi^0$$

is singled out from the events of (29). The data on $p\omega$ production will be considered in Section 10.4. It is clear from dN/dP_T^2 distribution for (31) (Fig.5) that in this reaction the coherent diffractive production process on carbon nuclei with the slope of diffractive cone $b \sim 50$ GeV^{-2} dominates in the region of small transverse momenta. The mass spectrum $M(p\eta)$ for all P_T^2 is presented in Fig.15.

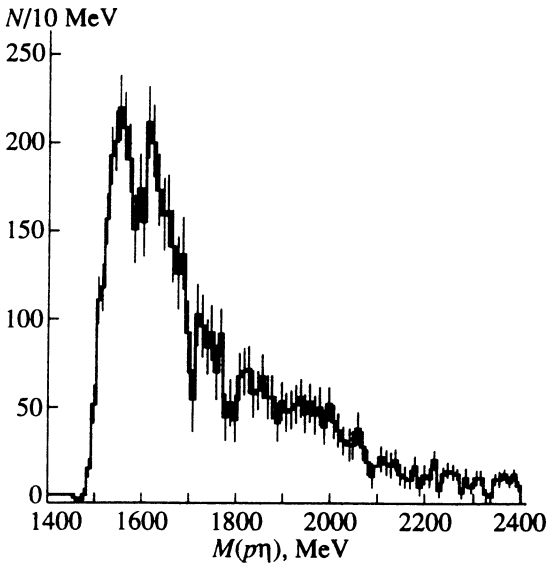

Fig. 15. The invariant mass spectrum $M(p\eta)$ for the reaction $p + N \rightarrow [p\eta] + N$ (31) for all P_T^2.

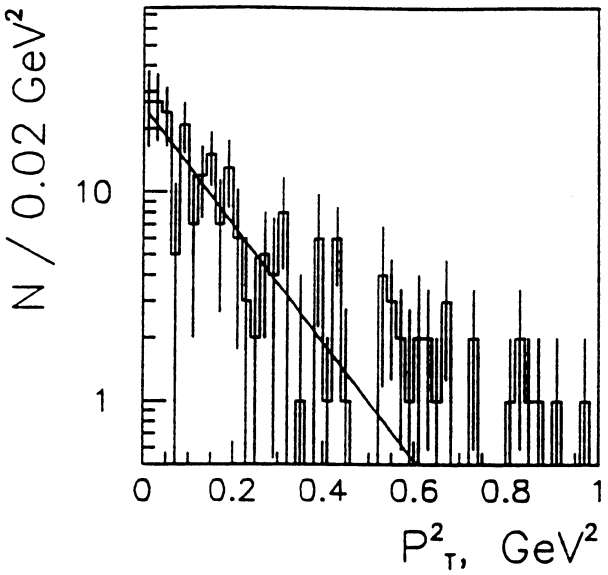

Fig. 16. dN/dP_T^2 distribution for the reaction $p + N \rightarrow [p\eta'] + N$ (32). In this distribution there is no evidence of coherent diffractive production (no forward peak with slope $b \geq 50$ GeV^{-2}). The slope of the distribution in the region of $P_T^2 < 0.5$ GeV^2 is $b \simeq 6.5$ GeV^{-2}.

The reaction

$$p + N \rightarrow [p\eta'] + N, \quad (32)$$
$$\hookrightarrow \pi^+\pi^-\eta$$

is also separated from the events of (30) (see Fig.4f) for the mass spectrum of $\pi^+\pi^-\eta$ system). The dN/P_T^2 distribution for (32) is given in Fig.16. As is seen from this figure, reaction (32) is the only diffractive- like production process studied by the SPHINX Collaboration (among more than a dozen of other reactions) in which one does not observe the strong coherent production on carbon nuclei (the absence of the forward peak in dN/dP_T^2 with a slope $b \sim 50$ GeV^{-2}). Thus the $p\eta'$ production reaction (32) is obviously a process of a nonperipheral character. It is instructive to compare Fig.16 with Fig.5 to demonstrate this phenomenon.

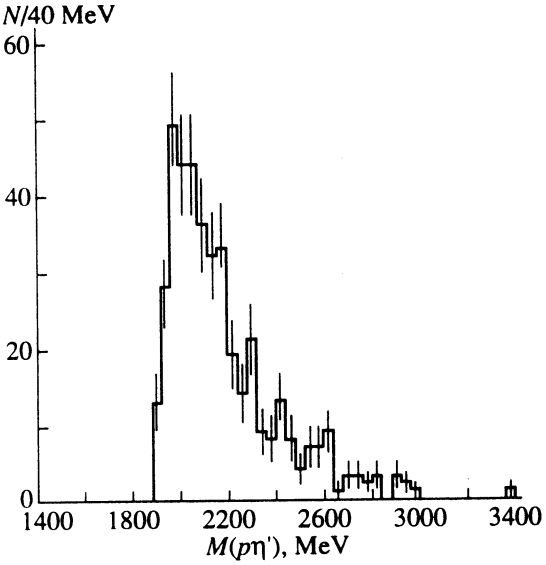

Fig. 17. The invariant mass spectrum $M(p\eta)$ for the reaction $p+N \to [p\eta'] + N$ (32) for all P_T^2.

The mass spectrum $M[p\eta']$ in (32) for all P_T^2 is presented in Fig.17. It is clear from Figs.15 and 17 that up to now only the first step in studying $[p\eta]$ and $[p\eta']$ systems was made. Further study of these very interesting systems requires a significant increase in statistics as well as more sophisticated data analysis. We hope to increase the number of events in the reactions under study by more than an order of magnitude in future runs with the completely upgraded SPHINX detector.

8. First data on the proton diffractive-like production in a nonperipheral domain [20,21]

As was discussed above, coherent diffractive production reactions seem to be quite promising processes to search for exotic hadrons, but, certainly, not the only ones. For instance, a nonperipheral production can be the most effective way to look for certain exotic states especially for those that are formed at short ranges. In this case the best conditions for the exotic hadron production are achieved at higher transverse momenta ($P_T^2 > 0.3 - 0.5$ GeV^2), where the background from peripheral processes is strongly suppressed. For instance, non-typically narrow meson states $X(1740) \to \eta\eta$ [35] and $X(1910) \to \eta\eta'$ [36] were observed in a study of the charge-exchange reactions $\pi^-p \to [\eta\eta] + \Delta^0$ and $\pi^-p \to [\eta\eta'] + n$, after the selection of events with $P_T^2 \geq 0.3$ GeV^2. These anomalous states are good candidates for cryptoexotic mesons. A mechanism of multiple rescattering with the Pomeron exchange (a gluon rich process) may explain the $X(1740)$ and $X(1910)$ production [37].

Searches for new baryons in the proton-induced diffractive-like reactions at high P_T^2 also seem to be quite promising [20,21]. Here we present the first (very preliminary) results on the invariant mass spectra of the $(\Sigma^0 K^+)$ and $(p\eta)$ systems produced in the

reactions $p + N \to [\Sigma^0 K^+] + N$ (10) and $p + N \to [p\eta] + N$ (31) with $P_T^2 > 0.3$ GeV^2. Combined data for the reaction (10) from the old and new runs are shown in Fig.18a. The data from the old run for reaction (31) are shown in Fig. 18b. Despite the limited statistics, a structure with the mass $M \approx 2350$ MeV and the width $\Gamma \sim 60$ MeV can be clearly seen in these two mass spectra. They require a further study in future experiments with large statistics. The same statement seems also to be true for an intriguing data on the invariant mass spectrum $M(p\eta')$ for reaction (32) in the region of $P_T^2 > 0.3$ GeV^2 presented on Fig.19.

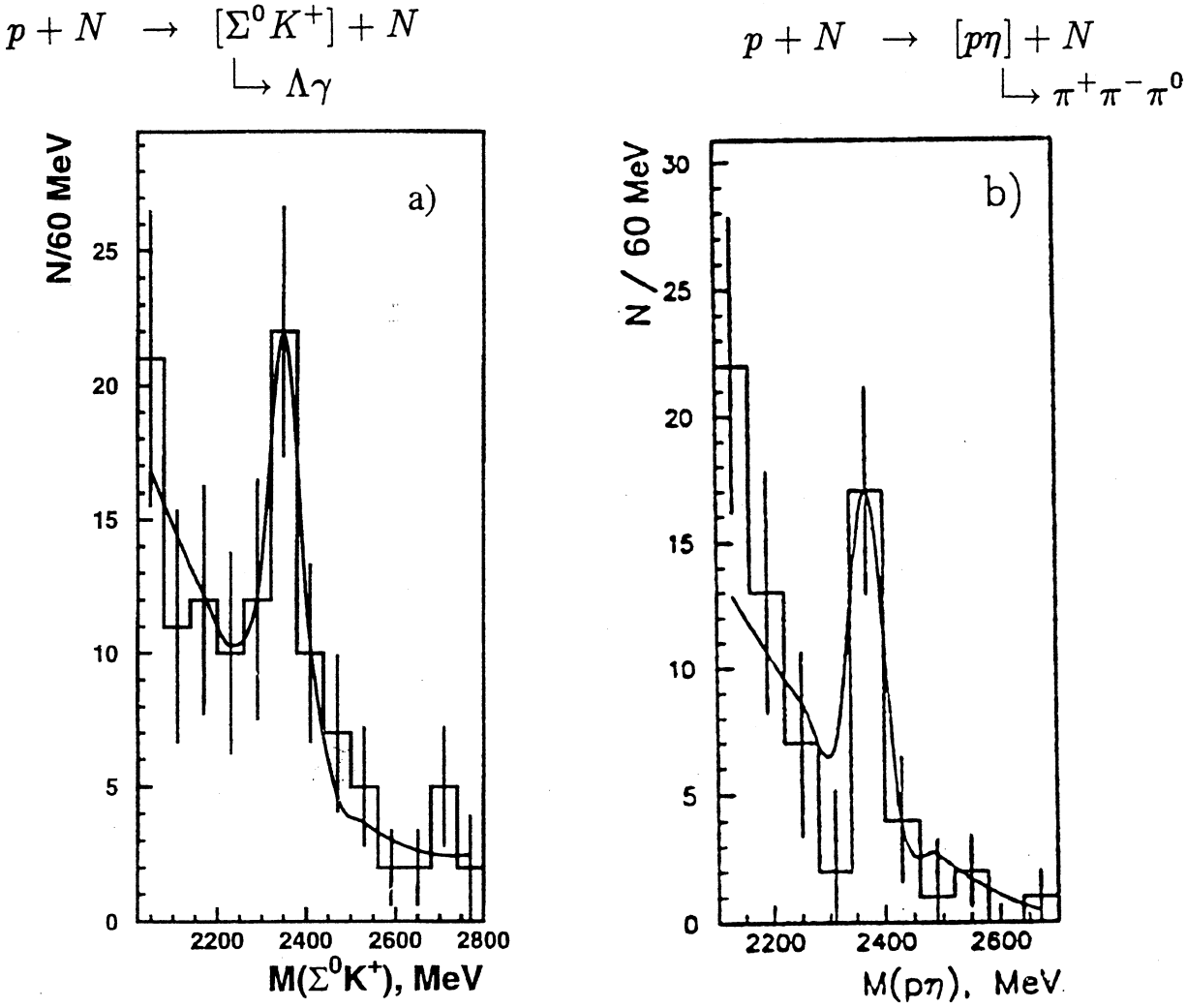

Fig. 18. a) Invariant mass spectrum of the $(\Sigma^0 K^+)$ system produced in the reaction $p + N \to [\Sigma^0 K^+] + N$ (10) at $P_T^2 > 0.3$ GeV^2 (combined data from the old and new runs). b) Invariant mass spectrum of the $(p\eta)$ system produced in the reaction $p + N \to [p\eta] + N$ (31) at $P_T^2 > 0.3$ GeV^2 (old data, see [20]). A narrow structure with $M \sim 2350$ MeV and $\Gamma \sim 60$ MeV in the non-peripheral region of (10) and (31) is seen in these mass spectra.